Journal of Directed Energy, **3**, Summer 2010, 304–319

Use of a Finite Element/Cohesive Zone Hybrid Method for Predicting the Failure of Structural Panels Irradiated by a Laser Source

Valmiki K. Sooklal,* Michael C. Larson, and Jesse McClure
Department of Mechanical Engineering, University of Colorado at Colorado Springs,
1420 Austin Bluffs Parkway, Colorado Springs, Colorado 80918

A computational finite element/cohesive zone hybrid method is used to simulate the fracture failure of structural panels that are irradiated by a laser source. Results from the computations are compared to those of experiments of laser irradiation from a CO_2 laser beam on pretensioned 2014 T6 aluminum specimens. Modified middle tension dogbone geometry specimens are subjected to a displacement-controlled boundary condition during irradiation. An iterative technique is employed that allows the key parameters used in the constitutive model for the cohesive elements to be related to the thermal field induced by the laser. The resulting computational technique accurately predicted the crack initiation and propagation in specimens subjected to a 200-W continuous beam. Peak temperatures in the range of 258°C were realized prior to failure.

KEYWORDS: Laser irradiation, Temperature-dependent cohesive elements, 3D finite element analysis, 2014 T6 aluminum

Nomenclature

a	half-length of embedded crack
L_c	cohesive element length, mm
t	effective (Cauchy) traction
$t_{\max}$	maximum traction
W_c	width of quarter symmetric panel
δ	effective displacement
δ_c	critical displacement
$\delta_{\max}$	maximum displacement
Γ_c	work of separation
σ_c	peak traction
φ	free energy potential function

Received January 20, 2010; revision received May 3, 2010.
*Corresponding author; e-mail: vsooklal@eas.uccs.edu.

1. Introduction

Lasers find wide use in a variety of industrial application and are well characterized for cutting and processing applications in which high precision and efficiency are key requirements. However, the deformation and failure mechanisms, fracture in particular, occurring in prestressed structures due to laser-induced heating are less well understood. When materials are subjected to intense levels of laser radiation beyond the range useful for controlled processing operations, complicated physical and mechanical phenomenon such as melting, vaporization, and electrodissociation can occur.[8] This work describes a new approach for computationally modeling the fracture failure of structural panels under such conditions.

Failure prediction under such extreme loading conditions is made difficult by rapid changes in the material that occur in the heat-affected zone due to the localized deposition of energy. Finite element analysis techniques have been used to predict the failure of materials that are irradiated by high-power lasers under certain conditions. For example, Keshun and Zheng[3] considered both numerical and theoretical models for the thermal buckling of axially precompressed cylindrical shells irradiated by a high-power laser. Although the numerical results agreed favorably with theoretical results for simple loading scenarios, they compared poorly with the actual experimental data. A significant issue is the macroscopic plastic deformation accompanying the change in ductility that occurs due to the rapid heating.

A continuum damage mechanics approach was used by Wei and Batra[7] when considering the deformation of an axially loaded thermoviscoplastic bar due to laser heating. Their analysis involved several assumptions that greatly simplified the problem in an attempt to provide a fundamental understanding of the processes involved in predicting failure. Admittedly, a thorough analysis of the problem required the use of numerical techniques, which was outside the scope of their study.

Apart from the heating, melting, and vaporization that occur during laser heating, as previously described, numerous other mechanical phenomena such as thermal stress, stress waves, and thermal shock will also appear. If the material is also under the action of a mechanical load, there will also be deformation and cracking.[2] This study is aimed at understanding the mechanisms of fracture failure through the use of three-dimensional (3D) finite element modeling software to better predict the failure of aluminum alloys under uniaxial loading while subjected to irradiation by a CO_2 laser.

It is proposed that a 3D, hybrid finite element/cohesive zone computational approach be used to simulate the mechanical response due to the heating effects of a CO_2 laser on 2014 T6 aluminum alloy panel specimens. The finite element software WARP3D[1] is adapted to achieve this result. This study implements a technique that augments the capabilities of WARP3D to account for a temperature gradient within the cohesive zone.

2. Laser Irradiation Experiment

The basic components for the laser irradiation experiment consist of a CO_2 laser, tensile testing machine, and high-speed video and thermal imaging cameras, as shown in Fig. 1. The laser used in these tests had a maximum power output of 700 W in continuous mode. A tensile testing machine having a maximum loading capacity of 50 kN was used to apply a displacement boundary condition to the specimens. Specially designed grips were needed for clamping thin specimens in order to apply yield level stresses without tearing or imposing appreciable deformation at the point of contact.

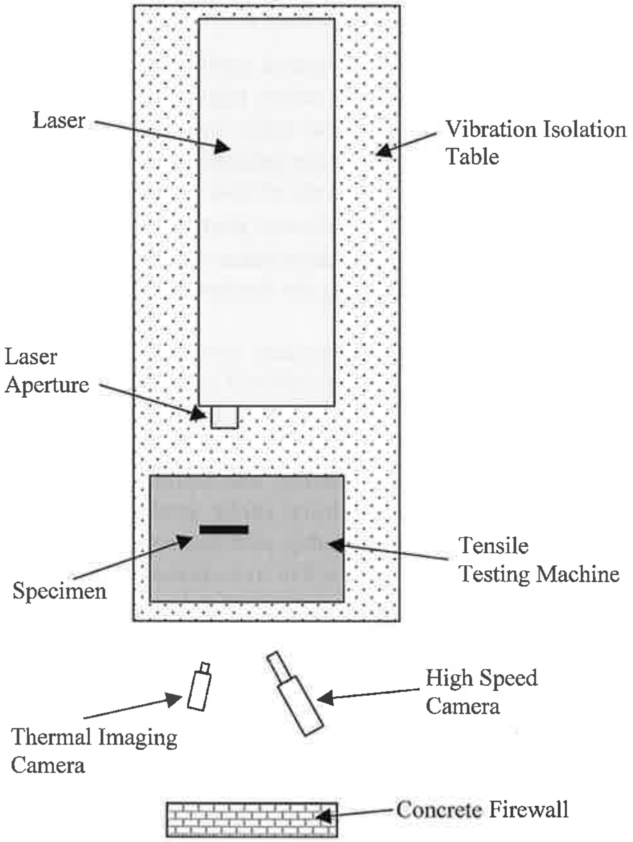

Fig. 1. Layout of laser testing apparatus.

A high-speed camera is used for capturing the failure event while the temperature profile produced by laser irradiation is acquired with the aid of a thermal imaging camera. The experiments performed in this study required specimens of a specific geometry. A modified middle tension dogbone specimen having the dimensions shown in Fig. 2 was laser cut from 2014 T6 aluminum alloy sheets, having a nominal thickness of 1.6 mm (0.063 in.).

The surface of the aluminum alloy used for testing is roughly 98% reflective. To ensure that the irradiated surface absorbed as much of the incident radiation as possible, a high-temperature matte black paint coating rated to withstand temperatures up to 650°C (1,200°F) was applied to the bare surface of the specimens. This provides increased coupling of incident radiation to the underlying metal surface as well as increasing the specimen's emissivity, which is particularly important when using thermal imaging equipment for gathering the temperature profile data during testing.

The test procedure involves mounting the painted specimen within the tensile test frame using the specially designed grips and applying displacement at a rate of 15 mm/min to the top surface of the specimen. The laser shutter is simultaneously opened at the instant the displacement boundary condition is applied. The high-speed and thermal imaging cameras simultaneously capture data during testing.

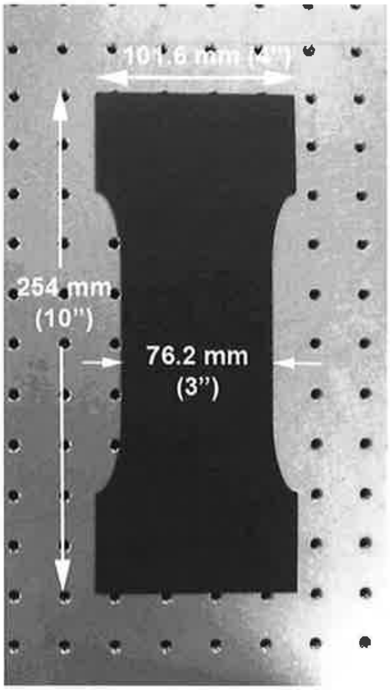

Fig 2. Image showing dimensions of a painted 2014 T6 aluminum dogbone specimen used for testing.

3. Cohesive Zone Model

The cohesive model idealizes the fracture process in solids as occurring within thin layers confined by two adjacent virtual surfaces. Crack formation/extension occurs due to a progressive decay of otherwise intact tractions and shear stresses across these adjacent surfaces, resulting in a loss of cohesion and subsequent crack propagation.[4]

An exponential relationship between the effective traction (t) and the effective displacement (separation) (δ) defines the traction-separation law and provides a phenomenological, decohesion model. This model constitutes all the features of the separation process by the following:

(1) the shape of the cohesive traction-separation curve ($t - \delta$),
(2) the local material strength defined by the peak traction (σ_c), and
(3) the local material ductility defined by the work of separation (Γ_c), given by the area under the $[(t - \delta)]$ curve.

The constitutive relation for the cohesive surface is derived from an exponential form for the free energy potential:

$$\phi = e\sigma_c\delta_c\left[1 - \left(1 + \frac{\delta}{\delta_c}\right)\exp\left(-\frac{\delta}{\delta_c}\right)\right], \tag{1}$$

where $e = \exp(1)$ and δ_c denotes the value of δ at $t = \sigma_c$. The constitutive relation for the cohesive surface derived from this potential follows an irreversible path with unloading

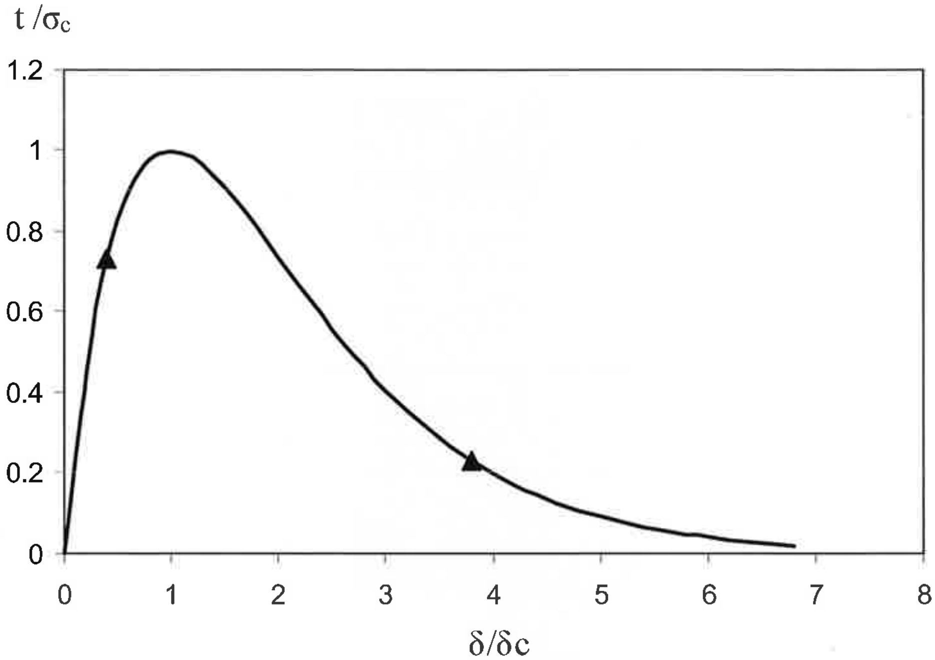

Fig. 3. Cohesive model for mode I growth expressed in terms of true (Cauchy) traction t and opening displacement δ for loading.

always directed toward the origin. Under loading conditions, the relationship between the true traction t and the normal displacement jump δ follows the form

$$t = \frac{\partial \phi}{\partial \delta} = e\sigma_c \frac{\delta}{\delta_c} \exp\left(-\frac{\delta}{\delta_c}\right). \tag{2}$$

When $\delta \leq \delta_{\max}$, the response for loading and reloading follows

$$t = \left(\frac{t_{\max}}{\delta_{\max}}\right)\delta. \tag{3}$$

Figure 3 shows loading responses predicted by the exponential form of the cohesive traction-separation law described here.

The interface cohesive elements used here for large displacement analyses consist of two four-node bilinear isoparametric surfaces that connect the congruent, bilinear faces of two adjacent isoparametric solid elements.[5] As the solid elements deform, the interface element undergoes relative displacement that generates tractions that follow the nonlinear traction separation given by Eq. (2).

The finite element code WARP3D was selected as the computational foundation for this study. It is a research tool designed to solve 3D solid models that are subjected to static and dynamic loads. The code has features that make it particularly attractive for investigating ductile fracture in metals, such as a library of isoparametric elements including interface-cohesive elements, a robust finite strain formulation, nonlinear material models, automatic adaptive solution strategies to enhance convergence, and very fast sparse direct solvers adapted for specific hardware platforms. The key advantage offered by WARP3D stems

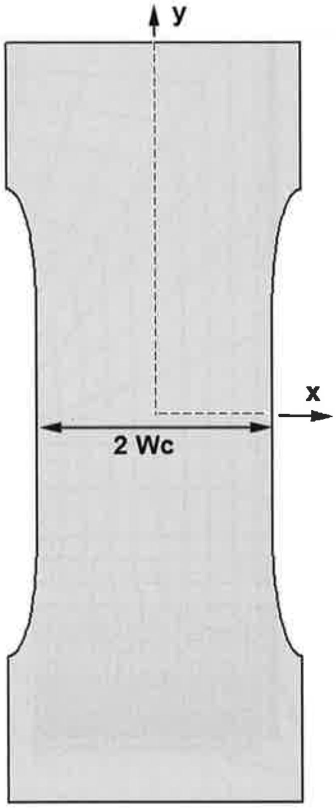

Fig 4. Middle tension M(T) dogbone specimen geometry.

from the technique used for simulating crack growth, which involves the use of interface cohesive elements. The use of element extinction procedures in the code allows the interface cohesive element to be removed from the model for each increment of crack growth, once the effective traction on the element reaches a very small value. As a result, remeshing is not required, allowing the local fracture process to evolve as a natural outcome of the computations. The constitutive models incorporated into the code assume isothermal conditions, so iterative modifications to the key material properties are required to allow the model to account for the imposed temperature field generated by the laser.

4. Finite Element Model for Laser Experiment

A dogbone-type middle tension geometry, shown in Fig. 4, was used for testing. To reduce computational time, a quarter symmetric model of this geometry (shown in Fig. 5) with appropriate boundary conditions was constructed using the finite element modeling (FEM) software Patran. This model has four elements through its thickness. There are 608 (152 × 4) eight-node bilinear isoparametric interface cohesive elements located along the symmetry plane $y = 0, 0 < x > W_c$.

These elements have a uniform length, $L_c = 0.25$ mm, and a thickness of 0.40 mm. Connected to these interface elements is a layer of eight-node hexagonal (Hex8) brick elements totaling 608 (152 × 4). Twelve-node hexagonal (Hex12) transition brick elements

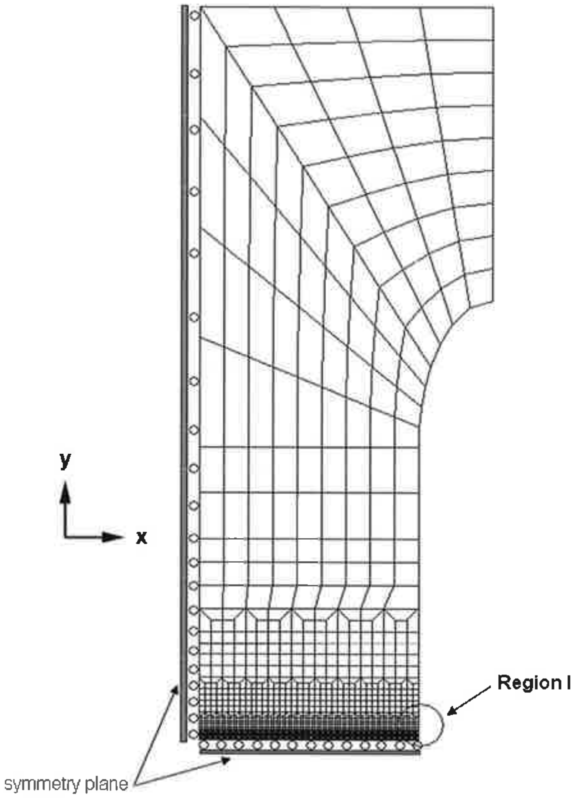

Fig. 5. Quarter symmetric model showing finite element mesh used in laser irradiation analysis.

connect these Hex8 elements to 20-node hexagonal (Hex20) brick elements, which are used to model the bulk material in the rest of the geometry. Figure 6 shows a detailed section of the mesh and outlines the layout of the various elements described in the model. The final model has 5,664 elements and a total of 24,291 nodes.

Prior to performing the calibration tests, a series of tests were done on the standard dogbone specimen shown in Fig. 2 to determine the yield stress and modulus of elasticity for temperatures of 22, 100, 200, 300, and 400°C with the aid of an environmental chamber. A total of three tests were performed at each temperature setting. These temperature-dependent mechanical properties were used to model the bulk material and are included in Table 1. Coefficient of linear expansion data for 2014 T6 aluminum were obtained from Touloukian and Ho.[6]

5. Calibration Model

The cohesive zone model used for the finite element simulation of the laser-irradiated dogbone specimens requires two key parameters to define the traction-separation law and the resulting decohesion process. These are the peak (effective) stress σ_C and the effective separation at peak stress δ_C. However, these two parameters function only for isothermal loading conditions. As such, there is no specific means of incorporating the effects of

Table 1. Summary of temperature-dependent material properties for 2014 T6 aluminum alloy

Temperature (°C)	Modulus of elasticity (GPa)	Yield stress (MPa)
22	73	414
100	71.45	404
200	69.87	328
300	57.06	133
400	40.77	29.5

temperature due to irradiation by the CO_2 laser into the analysis. To overcome this limitation, an alternative approach has been developed to appropriately model the compliance of these interface cohesive elements when they are subjected to a temperature field. In this approach an experimental calibration procedure is developed in conjunction with the appropriate cohesive zone finite element model.

The data obtained from these tests and simulations were then used to calibrate the finite element model used for the laser experiment with the new temperature-dependent cohesive parameters. The geometry for the specimens used in the calibration experiments is identical to that described for the laser model except that the specimens have a 4-mm crack machined at the center. Figure 7 shows a sketch of the specimen with the embedded crack. A one-eighth symmetric finite element cohesive model, shown in Fig. 8, was developed for the calibration simulations. Details of region II containing the crack are given in Fig. 9. The model has two elements through its thickness. There are 288 (144 × 2) eight-node bilinear isoparametric

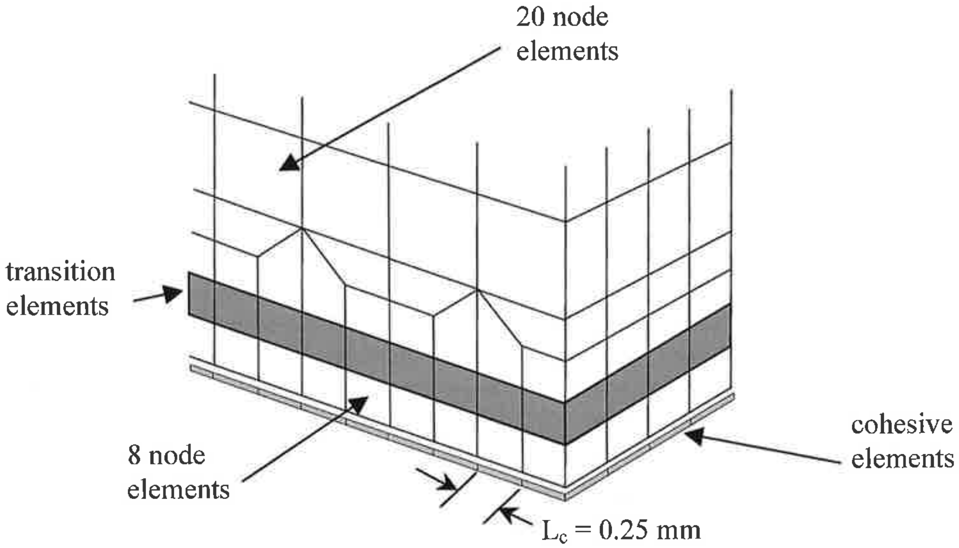

Fig. 6. Close-up of region I showing interface-cohesive elements located along the crack plane.

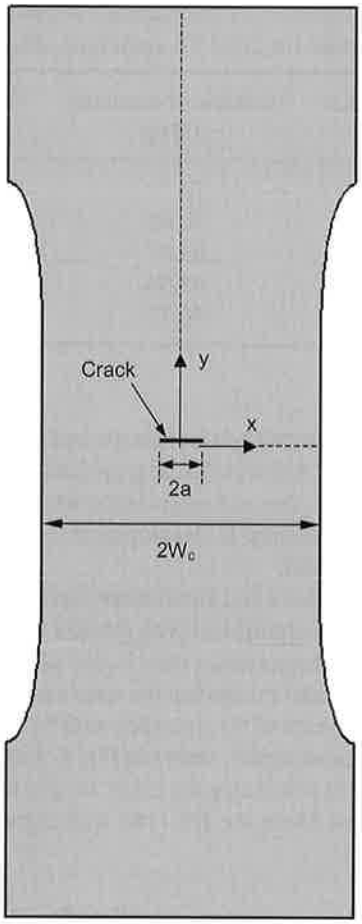

Fig 7. Middle tension M(T) dogbone specimen geometry with embedded crack.

interface cohesive elements along the symmetry plane $y = 0$, $a < x < (W_c - a)$, that are used to define the remaining uncracked portion of the specimen.

These elements have a uniform length, $L_c = 0.25$ mm, and a thickness of 0.40 mm. Connected to these interface elements is a layer of eight-node hexagonal (Hex8) brick elements totaling 304 (152×2). Twelve-node hexagonal (Hex12) transition brick elements connect these (Hex8) elements to 20-node hexagonal (Hex20) brick elements, which are used to model the bulk material in the rest of the geometry. The entire model has a total of 2,816 elements and 14,059 nodes. As the geometry is loaded in uniaxial tension, the cohesive elements deform until the critical displacement δ_c is attained. Once this occurs, the element is eliminated, allowing the crack front to further propagate.

To obtain temperature-dependent values for the cohesive parameters, a separate set of calibration experiments were performed at different temperatures. Dogbone specimens having geometry and dimensions identical to those used in the laser experiments were laser cut from a 2014 T6 sheet of aluminum having a nominal thickness of 1.6 mm (0.063 in.). A 4-mm crack was then machined at the center of each specimen. A total of three standard

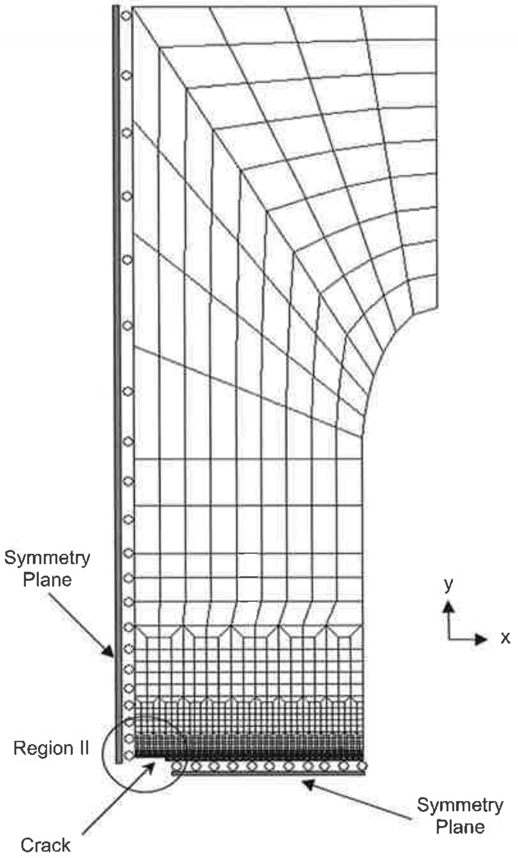

Fig. 8. One-eighth symmetric model showing finite element mesh used for calibration simulations.

tensile tests were performed on these specimens at each of the temperatures 150, 200, 250, and 300°C with the aid of an environmental chamber. The upper edge of the specimen was subjected to a fixed rate of displacement at 2 mm/min. The high-speed camera was used to capture the resulting crack growth until failure. The numerical model was then used to simulate the crack extension observed experimentally for the various temperatures by varying the peak stress σ_C and critical displacement δ_C until reasonable results were obtained. For relatively low-toughness materials experiencing initial ductile crack growth under small-scale yielding conditions, Γ_c can be estimated from measured values of the stress intensity factor K_c at the onset of stable ductile tearing using

$$\Gamma_c = \frac{K_c^2}{E^*}, \tag{4}$$

where E^* represents the effective Young's modulus for plane stress or plane strain.[5] To estimate an initial value for the peak stress σ_c, the yield stress data from the tensile test are used in the following equation:

$$\sigma_c = C\sigma_{ys}, \tag{5}$$

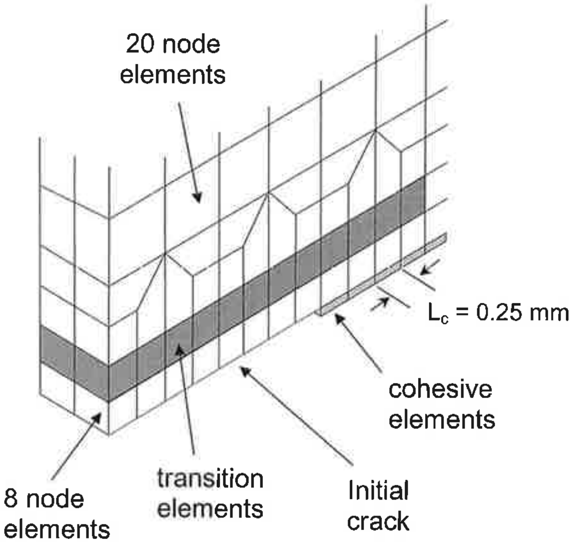

Fig. 9. Close-up of region II showing interface-cohesive elements and initial crack for calibration model.

where C is a constant and σ_{ys} is the yield stress at the selected temperature. Once σ_c is chosen, the corresponding δ_c is determined using the equation

$$\Gamma_c = e\sigma_c\delta_c. \tag{6}$$

A series of simulations are then performed in which the peak stress is varied until an optimum value is obtained. Once this is achieved, the value of σ_c is fixed and a second set of simulations are performed to determine the corresponding optimal value for δ_c. This process is then repeated for the 200, 250, and 300°C tests.

Figure 10 shows calibration plots for a peak stress optimization simulation at temperatures of 200°C. Figure 11 gives the calibration plots used for optimization of critical displacement δ_c for selected values of peak stress σ_c. The data obtained from these tests and simulations are then used to calibrate the final laser model with the new temperature-dependent cohesive parameters. Table 2 gives a summary of the optimum cohesive parameters obtained at the various test temperatures for which the calibration procedure was performed.

The thermograph data obtained from the thermal camera were used to produce a temperature profile of the beam that varies spatially, as shown in Fig. 12. This test was conducted using an output power of 200 W from the CO_2 laser. The temperature-dependent properties for the bulk material and cohesive elements are then assigned to the nodes and elements in the laser finite element model.

The material property assignment for the bulk material was accomplished by determining the nodal temperature and then computing the necessary values for modulus of elasticity, yield stress, and coefficient of linear expansion. These values were then assigned to each of the 23,531 solid element nodes. A separate code was written to relate the temperatures obtained from the thermal imaging camera to the nodal locations in the finite element model. This procedure allows the temperature field to be superimposed on the finite element structure, thereby allowing the measured temperature of the material to be related to the elements in the model. For the cohesive elements, the temperature of the midpoint of

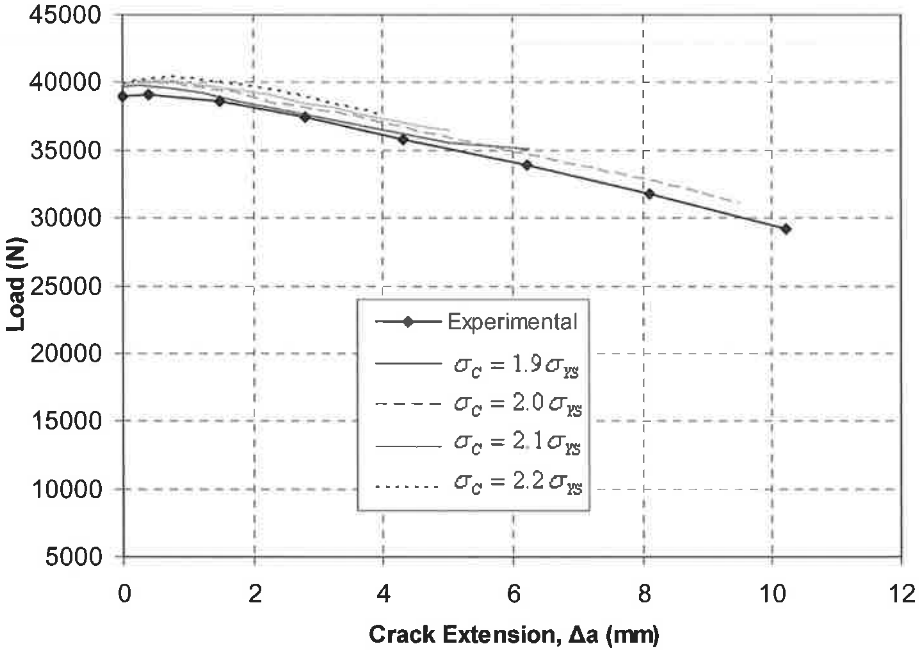

Fig. 10. Optimization of peak stress σ_c for 200°C.

the element is computed using the temperature profile data. The entire cohesive element is assumed to have a uniform temperature. The corresponding temperature-dependent cohesive parameters are then applied to each cohesive element. The effect of work hardening is accounted for using the strain hardening exponent in the WARP3D input file.

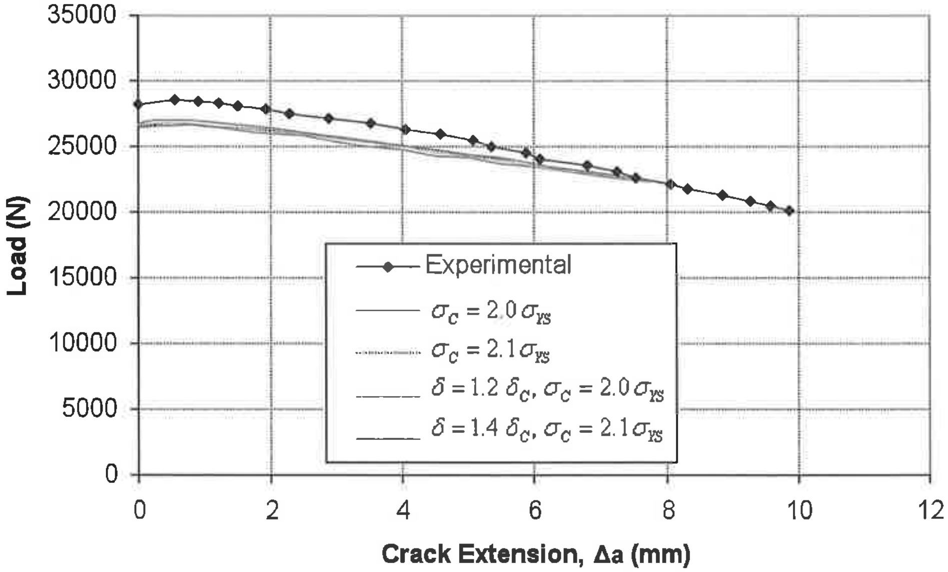

Fig. 11. Optimization of critical displacement δ_c for selected values of peak stress σ_c at 250°C.

Table 2. Summary of temperature-dependent cohesive parameters for 2014 T6 aluminum alloy

Temperature (°C)	Process zone (mm)	Peak stress σ_c (Nm^{-2})	Critical displacement δ_c (m)
150	1.76	7.320E+08	1.957E-05
200	1.57	6.560E+08	1.981E-05
250	0.93	4.230E+08	2.063E-05
300	—	2.793E+08	8.075E-06

6. Experimental and Computational Results

High-speed video image data for the laser test at 200 W were extracted and compared with the computational results obtained from the laser cohesive model. Figure 13 shows an image of the experimental results obtained for the 200-W test prior to the onset of unstable crack propagation. The peak temperature attained during this test was 258°C.

The cohesive model accurately predicts the process of crack nucleation and subsequent crack propagation. The crack forms at the same instant in the cohesive model as occurred in the actual test and at the same location. Five tests were performed on specimens at the 200- and 300-W power settings. The quantity of stable growth also appears to be closely matched, as the experiment records an average of 4 mm of crack extension, whereas the model predicts 3.75 mm of growth before the crack becomes unstable. It should also be noted that the time period of 17 s before unstable growth appears in the computational

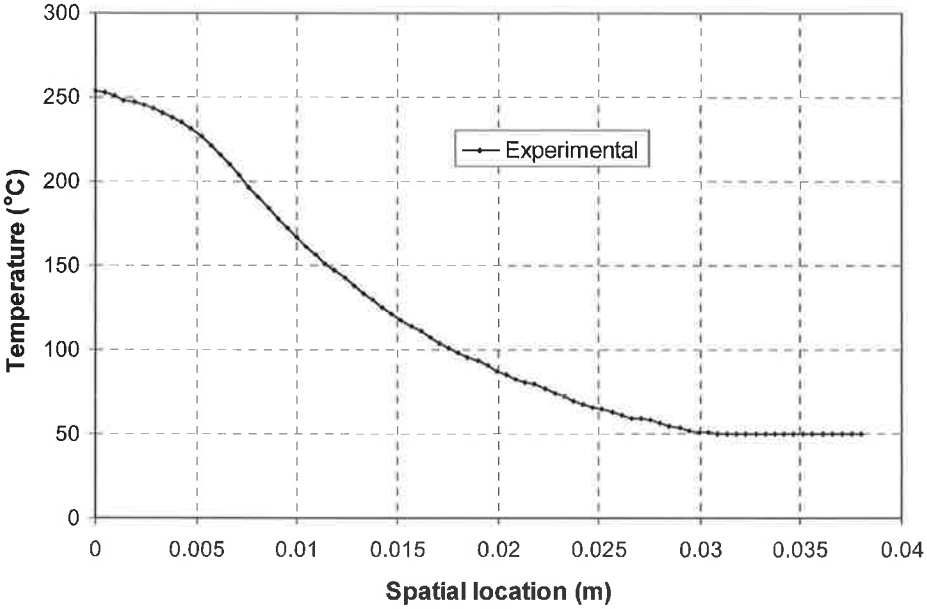

Fig. 12. Temperature profile for 2014 T6 aluminum specimen irradiated at a power output of 200 W at the instant of failure.

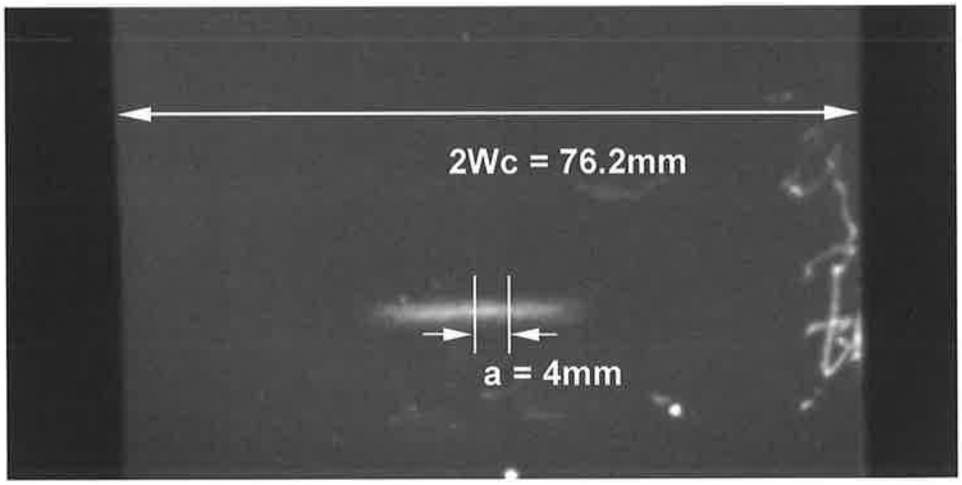

Fig. 13. High-speed video image of 2014 T6 specimen showing the maximum measurable crack length prior to unstable crack propagation from irradiation at an output power of 200 W.

model also matches very closely with the experimental time of 18 s after the start of the applied load. For the 300-W test, the peak temperature attained was 354°C. The simulations performed at this power level yielded less-accurate results, with the model predicting tearing occurring after 19 s as compared to 16 s in the actual test, for an average of 9 mm of stable crack growth. The cohesive model indicates that the elements in the vicinity of the irradiated zone at this temperature experience deformations that are too large to allow convergence to a reasonable solution. The model does predict substantial contraction of the specimen in the thickness direction due to the Poisson's effect in the heat-affected zone, as observed in the actual test.

The length of the crack that formed in the heat-affected zone is very small and difficult to measure during nucleation and subsequent crack propagation. When using our high-speed camera data (50,000 images per second), the resolution becomes very low, making it difficult to accurately define a clear crack front. As a result, obtaining experimental data for crack growth with time for comparison with model data did not seem to be feasible in this study. Instead, what was considered was the period of stable growth during the irradiation process and the maximum length measurable before the crack became unstable. This was then compared with the crack length provided by the model and the time taken for this event to occur in both cases.

7. Summary and Conclusion

A temperature-dependent cohesive zone model was developed to model the effects of laser irradiation on 2014 T6 aluminum specimens that were subjected to a displacement-controlled boundary condition at a rate of 15 mm/min. To make the cohesive elements (which are formulated for isothermal conditions) capable of handling a temperature field, a calibration technique was developed in which the key parameters needed for the interface elements were determined for temperatures of 150, 200, 250, and 300°C. For elements with temperatures within this range, the necessary parameters were determined through interpolation. Temperature-dependent material properties were assigned to the bulk material as well as the interface cohesive elements to more accurately simulate the heating effects of the laser on the specimen's compliance.

For 250°C, the cohesive zone model formulation used in the calibration simulations gives very acceptable results. Beyond 250°C, the numerical results progressively deviate from the experimental data obtained from the calibration tests.

Based on this finding, it appears that some threshold temperature does exist for developing a temperature-dependent interface cohesive zone model. The results obtained here are significant in two ways. First, they show that the technique outlined in this study can be used to calibrate the interface cohesive elements to allow for the effects of temperature in terms of failure prediction. Second, they establish an upper bound of approximately 270°C as the limit for which the cohesive model using the current constitutive formulation is applicable.

In conclusion, it can be said that for power levels up to and including 200 W (from a continuous CO_2 laser having a spot size of 14 mm), which generates peak temperatures in the range of 258°C before fracture, the temperature-dependent cohesive zone model developed in this study very accurately predicts the process of crack initiation and subsequent crack propagation. At temperatures above 270°C, the model's ability to predict failure begins to break down. This is primarily due to the fact that the material in the heat-affected zone softens considerably and becomes visco plastic, thereby making a solid element cohesive model formulation inappropriate in terms of failure prediction.

References

[1] Gullerd, A., K. Koppenhoefer, A. Roy, S. RoyChowdhury, M. Walters, B. Bichon, K. Cochran, and R. Dodds, "WARP3D-Release, 15.3 3-D Dynamic Nonlinear Fracture Analysis of Solids Using Parallel Computers and Workstations," Civil Engineering Studies, Structural Research Series No. 607, Department of Civil Engineering, University of Illinois at Urbana–Champaign (2004).

[2] Huimin, X.,W. Guotao, Z. Daqing, D. Fulong, P. Dietz, Z. Wei, and A. Schmidt, J. Mat. Proc. Technol. **82**, 137 (1998).

[3] Keshun, D., and J. Zheng, J. AIAA **38**(10), 1738 (2000).

[4] Roy, Y.A., and R.H. Dodds, Jr., Int. J. Fracture **110**, 21 (2001).

[5] Roychowdhury, S., Y.D.A. Roy, and R.H. Dodds, Jr., Eng. Fracture Mech. **69**, 983 (2002).

[6] Touloukian, Y.A., and C.Y. Ho, "Thermophysical Properties of Selected Aerospace Materials, Part II: Themophysics Properties of Screen Materials," Purdue University (1976)

[7] Wei, Z.G., and R.C. Batra, J. Therm. Stresses **26**, 701 (2003).

[8] Zhang, S., Y. Yin, G. Zhang, and Y. Chen, Key Eng. Mat. **177**, 99 (2000).

The Authors

Dr. Michael Larson is the El Pomar Endowed Chair of Engineering and Innovation and a Professor of Mechanical and Aerospace Engineering and serves as the Associate Vice Chancellor for Research at the University of Colorado at Colorado Springs. He earned his Ph.D. in mechanical engineering from MIT in 1992. His current research focus is on laser/materials interactions.

Mr. Jesse McClure is the Senior Designer at MIND Studios, a professional product design laboratory housed within the University of Colorado at Colorado Springs. He earned his Master's in mechanical engineering from Tulane University in 2005. His current research interests involve characterizing the effects of laser energy on nasal tissue for use in medical devices.

Dr. Valmiki K. Sooklal completed his Ph.D. at Tulane University in 2007. His research focused on laser/material interaction using carbon dioxide lasers and metals. He then accepted a position at the University of Colorado at Colorado Springs, where he continued with laser research. His focus changed from metals to investigating light scattering in tissue from a laser source and the subsequent effects of the thermal deposition of energy on protein structures within tissue. He is also involved in laser excitation and detection of wavelength-specific dyes for biological pathogen detection.